Theory of Chain Pull-Out and Stability of Weak Polymer Interfaces. 2

L. Kogan, C.-Y. Hui,* and A. Ruina

Department of Theoretical and Applied Mechanics, Cornell University, Ithaca, New York 14850

Received June 27, 1995; Revised Manuscript Received March 4, 1996[⊗]

ABSTRACT: In this paper, we study the relationship between crack nucleation and failure of an interface reinforced by chains and the results of a linear stability analysis presented in part 1 of this study (preceding paper in this issue). We develop a numerical procedure to simulate the deformation and failure of such an interface. We demonstrate that instabilities lead to spatial localization of the deformation which determines the failure mode of the interface. The dependence of the failure modes on the material parameters of the system, such as the number of entanglements of the pull-out chains, the level of applied load, and the amplitude of the initial perturbation, is studied.

1. Introduction

In part 1 of this work, we examined the linear stability of an interface reinforced by polymer chains.[1] The deformation of the interface is assumed to be governed by a chain pull-out mechanism. Our stability analysis indicates that spatially homogeneous solutions are unstable with respect to perturbations which have long wave components in their Fourier spectrum.

The linear stability results in part 1 of this work are strictly valid only when the amplitude of inhomogeneous interface displacement is small compared with the homogeneous solution. In other words, these results are limited to sufficiently short times and, thus, cannot be used to study the problem of crack initiation and the subsequent failure of the interface.

In part 2 of this work, the time evolution of the instability due to a random initial spatial perturbation is studied by the numerical integration of the governing equations for the special case of an elastic half-space bonded to a rigid substrate. The numerical procedure we developed allows us to simulate the complete failure of the interface. To the best of our knowledge, there has been no previous work done on the numerical simulations of crack nucleation and failure of a spatially homogeneous polymer interface. The first part of this work focused on crack initiation. We first deduce the regions of validity of our linear stability analysis by comparing the results of numerical simulations with the results of the linear stability analysis in part 1. The dependence of crack initiation and the failure modes of the interface on loading and microstructural parameters is then explored.

The following notations for citing equations will be used in this work. Equations in part 1 will be referred to as eq 1.*xx*, where *xx* is the equation number. For example, eq 1.12 is eq 12 in part 1. Likewise, eq 5 in part 2 will be referred to as eq 2.5.

2. Numerical Solution Procedure

As in part 1, we consider the case of an elastic half-space ($y > 0$) bonded to a rigid half-space ($y < 0$) as shown in Figure 3 of part 1. The deformation of the interface, for $\dot{\delta} > 0$ and $\delta < \Delta$, is governed by eq 1.5 of part 1; i.e.,

$$\sigma = B\mathrm{e}^{C(\Delta-\delta)}\dot{\delta} \tag{2.1a}$$

where σ is the normal interface traction, δ is the interface opening displacement, Δ is the critical interface opening, and B and C are material parameters defined in part 1 (see eqs 1.2 and 1.3). To account for the fact that the pull-out force must approach zero as a chain is completely pulled out, eq 2.1a can be modified by replacing $\mathrm{e}^{C(\Delta-\delta)}$ by $\mathrm{e}^{C(\Delta-\delta)}-1$ (see eq 1.17):

$$\sigma = B[\mathrm{e}^{C(\Delta-\delta)} - 1]\dot{\delta} \tag{2.1b}$$

Note that we have set $\sigma^* = 0$ in eq 2.1 where σ^* is the stress needed to initiate pull-out.

Following the same procedure as in part 1 of this work, the normalized governing equation for the evolution of an interface subjected to the stress in eq 2.1b is found to be

$$\tilde{\sigma}^{\mathrm{elastic}}(u) + 1 = (\mathrm{e}^{-u} - \mathrm{e}^{-A})\frac{\partial u(t',x')}{\partial t'} \qquad u < A \tag{2.2a}$$

$$\tilde{\sigma}^{\mathrm{elastic}}(u) + 1 = 0 \qquad u \geq A \tag{2.2b}$$

where $u(x',t')$ is a normalized interface opening. x' and t' are the normalized spatial and temporal coordinates, defined by eq 1.23; i.e.,

$$t' = \frac{\sigma_\infty C}{Be^A}t$$

$$x' = \frac{\sigma_\infty C(1-\nu)}{G}x$$

$$u(t',x') = \frac{A}{\Delta}\delta(t,x)$$

$$\tilde{\phi}(u) = \mathrm{e}^{-u} - \mathrm{e}^{-A}$$

$$\tilde{\sigma}^{\mathrm{elastic}}(u) = \frac{1}{\pi}\int_{-\infty}^{\infty}\frac{u_{,\xi'}(t',\xi')}{\xi' - x'}\,\mathrm{d}\xi' \tag{2.3}$$

$$A = C\delta = \mu s/s_{\mathrm{e}}$$

We will omit the primes in the notation for the normalized spatial and temporal coordinates when it does not lead to confusion. The normalized elastic operator $\tilde{\sigma}^{\mathrm{elastic}}(u)$, which was given by eq 1.20f, can be rewritten

[⊗] Abstract published in *Advance ACS Abstracts,* May 1, 1996.

S0024-9297(95)00908-9 CCC: $12.00

in the following form:

$$\tilde{\sigma}^{\text{elastic}}(u(t,x)) = \int_{-\infty}^{\infty}(-|\kappa|)u(t,\kappa)e^{i\kappa x}\,d\kappa \qquad (2.4)$$

where

$$u(t,\kappa) = \frac{1}{2\pi}\int_{-\infty}^{\infty}u(t,x)e^{-i\kappa x}\,dx$$

is the Fourier transform of $u(t,x)$. Equation 2.4 can be obtained by noting that the interface opening displacement $u(t,x)$ is related to $u(t,\kappa)$ by the inverse Fourier transform; i.e.,

$$u(t,x) = \int_{-\infty}^{\infty}u(t,\kappa)e^{i\kappa x}\,d\kappa$$

By using eq 1.27 and the relation $\lambda(\kappa) = -|\kappa|$, we found

$$\sigma^{\text{elastic}}(u(t,x)) = \sigma^{\text{elastic}}\left(\int_{-\infty}^{\infty}u(t,\kappa)e^{i\kappa x}\,d\kappa\right) = \int_{-\infty}^{\infty}u(t,\kappa)\sigma^{\text{elastic}}(e^{i\kappa x})\,d\kappa = \int_{-\infty}^{\infty}u(t,\kappa)(-|\kappa|e^{i\kappa x})\,d\kappa$$

We simulate the behavior of the infinite interface by computing the evolution of the interface opening $u(t,x)$ on a finite portion of the interface of length L. The spatial coordinate is discretized using a uniform mesh with N nodes located at x_i. The spacing Δx between nodes is $\Delta x = L/N$. At any time t, the displacement $u(t,x)$ and the normal traction $\tilde{\sigma}^{\text{elastic}}(t,x)$ on the interface are specified by their discretizations:

$$\mathbf{U}(t) \equiv (u(t,x_1),...,u(t,x_N))$$

$$\sigma(t) \equiv (\tilde{\sigma}^{\text{elastic}}(t,x_1),...,\tilde{\sigma}^{\text{elastic}}(t,x_N))$$

To avoid end effects in the numerical simulation, we seek solutions that are periodic in space with period L. We have carried out numerical simulations using different periods to ensure that the results of the discrete system do not depend on the length of the period we used in our analysis. Details of these simulations are given in the Appendix. This means that our solution has all the important quantitative features of the solution for the infinite interface problem.

Equation 2.2a governs pull-out prior to crack nucleation; i.e., $\delta < \Delta$ or $u < A$. To solve eq 2.2a, we obtain a discrete version of the elastic operator $\tilde{\sigma}^{\text{elastic}}(u)$, eq 2.4, using a fast Fourier transform (FFT) algorithm. This approach allows us to transform the displacement vector $\mathbf{U}(t)$ with N components

$$\mathbf{U}(t) \equiv (u(t,x_1),...,u(t,x_N)) \xrightarrow[FFT]{} (\tilde{\sigma}^{\text{elastic}}(t,x_1),...,\tilde{\sigma}^{\text{elastic}}(t,x_N)) \equiv \tilde{\sigma}(t)$$

to a vector $\tilde{\sigma}(t)$ with N components approximating the values of the stress at the same nodes. This approach ensures that if the initial conditions for $u(t,x)$ are periodic with period L, $u(t,x)$ will also be periodic with period L throughout the stimulation. The discretized version of eq 2.2a is a system of ordinary differential equations (ODE's)

$$\frac{\partial u_i(t)}{\partial t} = (e^{-u_i} - e^{-A})^{-1}(\tilde{\sigma}^{\text{elastic}}(u)_i + 1) \qquad (2.5)$$

where the index i denotes the value of the corresponding function at node number i, namely, $f_i \equiv f(x_i)$.

The system of ODE's eq 2.5 is supplemented by an initial condition which is a random noise having a normalized amplitude

$$\epsilon' = A\epsilon \ll 1$$

where $A = \mu(s/s_e)$ is defined in eq 2.3 ($\mu \approx 15/8$). Specifically, the normalized opening displacement at $t = 0$ is assumed to be

$$u(t=0,x_i) = \epsilon'\tilde{g}(x_i) \qquad (2.6)$$

where $\epsilon' \ll 1$ and $\tilde{g}(x_i)$, $1 \le i \le N$, are independent random variables uniformly distributed between 0 and 1. The system of ODE's eq 2.5 with initial condition eq 2.6 is solved by a standard Runge−Kutta procedure. Since the solution of eq 2.2 depends only on two parameters, A and ϵ (or equivalently A and ϵ'), throughout the simulations we will study the dependence of the solution on the parameters A and ϵ or A and ϵ'.

The solution procedure just described will be referred to as procedure 1. It allows us to calculate the solution of eq 2.5 at all nodes x_i for $t < T_c$, i.e., before the nucleation of the first crack. Crack nucleation occurs at the normalized time T_c when the equality $u_i = A$ is satisfied at some point x_i of the interface. After the first crack nucleates, our numerical procedure must be modified to enforce the traction-free condition on the crack faces demanded by eq 2.2b.

To satisfy eq 2.2b when $u_i \ge A$, we use the following approach (procedure 2): suppose the solution $u(t,x_i)$ is known for all i, $1 \le i \le N$, and for $t \le t_j$ and that, at $t = t_j$, there exist some nodes such that $u_i \ge A$. To calculate $u(t,x_i)$ at $t = t_j + \Delta t$, we first use procedure 1 for all x_i such that $u(t,x_i) < A$; i.e., we solve the following system of ordinary differential equations:

$$\frac{\partial u_i(t)}{\partial t} = (e^{-u_i} - e^{-A})^{-1}(\tilde{\sigma}^{\text{elastic}}(u)_i + 1) \qquad u_i < A \quad (2.7a)$$

For those nodes with $u_i \ge A$, we integrate the equations

$$\frac{\partial u_i(t)}{\partial t} = \zeta^{-1}(\tilde{\sigma}^{\text{elastic}}(u)_i + 1) \qquad u_i \ge A \quad (2.7b)$$

where ζ is a small parameter. These two systems of eqs 27a,b are coupled and must be solved simultaneously. In actual simulations, ζ was taken to be 10^{-6}. In this way, we obtain a first approximation $u^1(t_j+\Delta t,x_i)$ to the solution. We expect that if ζ is sufficiently small, $\tilde{\sigma}^{\text{elastic}}(u^1)_i + 1 \approx 0$ for $u^1{}_i \ge A$ so that eq 2.2b is approximately satisfied. By using $u^1(t_j+\Delta t,x_i)$, we initiate an iteration procedure to satisfy eq 2.2b for all x_i such that $u^1(t_j+\Delta t,x_i) \ge A$. These iterations are performed according to the following scheme:

$$\frac{u^n(t_j+\Delta t,x_i) - u^{n-1}(t_j+\Delta t,x_i)}{\tau} = [\tilde{\sigma}^{\text{elastic}}(u^{n-1})](t_j+\Delta t,x_i) + 1 \qquad u \ge A \quad n \ge 2$$

$$u^n(t_j+\Delta t,x_i) = u^{n-1}(t_j+\Delta t,x_i) \qquad u < A \quad (2.7c)$$

where u^n denotes the nth approximation to the solution of eqs 2.5a,b. The iteration parameter τ is determined by numerical experiments to provide covergence. The criterion of convergence is

$$\max_{x_i}(|[\tilde{\sigma}^{\text{elastic}}(u^{n-1})](t_j+\Delta t,x_i) + 1|) \le 0.01 \quad (2.8)$$

If the iterations converge, a new increment in time is

taken and the procedure is repeated until the total failure of the interface occurs.

Numerical procedure 2 described above allows us to simulate the simultaneous propagation of several cracks along the interface without explicit determination of their locations. This is convenient because no modification of the numerical scheme is needed when new cracks nucleate or when two cracks link together (crack coalescence).

All the numerical simulations in this work are carried out with $L = 32(2\pi)$ and $N = 1024$. This choice of L and N is based on the numerical simulations using different periods to ensure that the results of the discrete system do not depend on the length of the period we used in our analysis. Details are given in the Appendix.

3. Results of Numerical Simulations

3.1.1. Development of Instability and Localization, $u \leq A$. The first set of numerical simulations is designed to study the development of instabilities and their relation to spatial localization before crack initiation. In this case, $u < A$ everywhere so that we need only consider the evolution of $u(t,x)$ before the nucleation of the first crack. We seek to compare our numerical solutions of the governing equations with the predictions of the linear stability analysis given in part 1.

In this set of numerical simulations, eqs 2.2a,b are replaced by a single equation

$$\tilde{\sigma}^{\text{elastic}}(u) + 1 = e^{-u}\frac{\partial u(t,x)}{\partial t} \tag{2.9}$$

This modification may be justified as follows: since we are interested in the case $u < A$, eq 2.2b is not needed. Also, when u is significantly smaller than A, $e^{-u} - e^{-A} \approx e^{-u}$. This modification is equivalent to using eq 2.1a as the interface model, i.e., $\sigma = Be^{C(\Delta-\delta)}\dot{\delta}$. The advantage of this modification is that a single simulation is needed to quantify the instability process for a given amplitude of the initial perturbation ϵ', since eq 2.9 is independent of A and the dependence of the solution on A appears only in the initial conditions, eq 2.6 (recall that $\epsilon' \equiv A\epsilon$). Thus, for any given A, the solution $u(t,x)$ before crack nucleation (i.e., $u \leq A$) is given by $u(t,x)$, $0 \leq t \leq T_c$, where T_c is defined by $u_{\max}(T_c,\epsilon') = A$. Note that $u(t,x)$, $0 \leq t \leq T_c$, is a good approximation of the solution of eq 2.2a for all values of t, except for $t \approx T_c$.

3.1.2. Dependence of Localization on the Amplitude of the Initial Perturbation. To see how localization develops, we calculate the following measure of localization:

$$\text{loc}(t,\epsilon') = \frac{\max_x(u(t,x;\epsilon'))}{\text{mean}_x(u(t,x;\epsilon'))} \tag{2.10}$$

where $\text{mean}_x(u(t,x;\epsilon'))$ is the spatial average of the interface opening displacement:

$$\underset{x}{\text{mean}}(u(t,x;\epsilon')) = \frac{1}{L}\int_0^L u(t,x;\epsilon')\,dx \tag{2.11}$$

Since $\text{loc}(t,\epsilon')$ is calculated using $u(t,x;\epsilon')$, it depends implicitly on the initial noise $\tilde{g}(x_i)$ and its amplitude ϵ'. This dependence is not indicated explicitly by the notation $\text{loc}(t,\epsilon')$. According to the definition given by eq 2.10, $\text{loc}(t,\epsilon') \geq 1$ for all values of t. For a spatially uniform interface opening (i.e., the homogeneous solution $u_0(t) = -(\log(1 - t))$ defined in part 1 of this work), $\text{loc}(t,\epsilon') \equiv 1$ so that deviation of $\text{loc}(t,\epsilon')$ from 1 measures localization. We can now study how the localization process depends on the amplitude of the initial perturbation by calculating $\text{loc}(t,\epsilon')$ for several solutions with the same initial noise $\tilde{g}(x')$ but different amplitudes ϵ'.

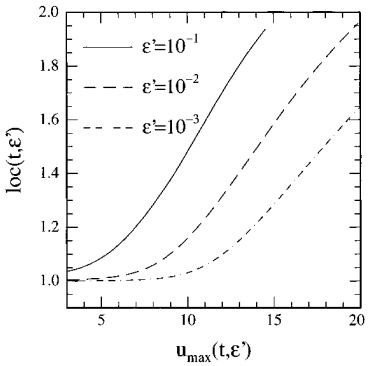

Figure 1. $\text{loc}(t,\epsilon')$ plotted against $u_{\max}(t,\epsilon')$ for $\epsilon' = 10^{-1}$, 10^{-2}, and 10^{-3}. ϵ' is the normalized amplitude of the initial perturbation in the interface opening defined by eq 1.24c. $\text{loc}(t,\epsilon')$ is the measure of spatial localization of the interface opening and is defined by eq 2.10. $u_{\max}(t,\epsilon')$ is the maximum value of the interface opening at time t, and it is a monotone increasing function of t.

Instead of plotting $\text{loc}(t,\epsilon')$ vs t, we plot $\text{loc}(t,\epsilon')$ vs the maximum opening displacement $u_{\max}(t,\epsilon')$, which is a monotonically increasing function of t. This plot is shown in Figure 1 where $\text{loc}(t,\epsilon')$ is plotted against $u_{\max}(t,\epsilon')$ for several different values of ϵ'. Figure 1 shows that $\text{loc}(t,\epsilon')$ is close to 1 for sufficiently small values of $u_{\max}(t,\epsilon')$ and has almost a zero slope. This means that there is no localization in the beginning of the pull-out process. When $u_{\max}(t,\epsilon')$ reaches certain critical values $u_c(\epsilon')$, which depends on ϵ', $\text{loc}(t,\epsilon')$ starts to increase and varies approximately linearly with $u_{\max}(t,\epsilon')$, indicating localization. The linear growth of $\text{loc}(t,\epsilon')$ after $u_{\max}(t,\epsilon') > u_c(\epsilon')$ is due to the fact that the average value of the interface opening does not change significantly compared to $u_{\max}(t,\epsilon')$ during the localization process. Thus, the condition $u_{\max}(t,\epsilon') = u_c(\epsilon')$ indicates the onset of localization. Figure 1 shows that $u_c(\epsilon')$ decreases as ϵ' increases so that the larger the amplitude of the initial perturbation, the earlier localization starts to develop. In physical terms, an increase in the entanglement number of pull-out chains or in the amplitude of the initial perturbation decreases the maximum relative opening displacement δ/Δ needed to develop spatial localization.

The explanation for this feature is as follows: localization develops due to the decrease in the resisting pull-out force on a portion of the interface. This decrease in the resisting pull-out force causes an increase in the rate of interface opening in this portion of the interface, which leads to a further decrease of the resisting pull-out force. Continuation of this process leads to localization. According to the chain pull-out model described by eq 1.1, the resisting pull-out force is related to the pull-out rate through the friction coefficient, which increases with the entanglement number. Consider two interfaces with chains of the same length but with different numbers of entanglements. To be specific, we will assume that chains in interface 1 have more entanglements than those in interface 2. The two interfaces are loaded in exactly the same way. Furthermore, the *same* perturbation of the interface opening is imposed on both interfaces. Consider a region of

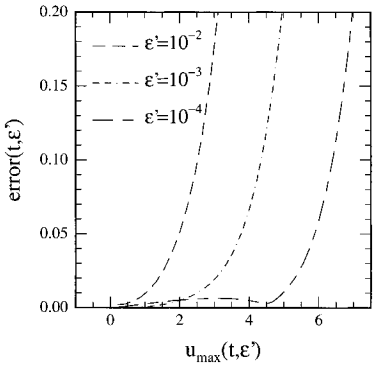

Figure 2. error(t,ϵ') plotted against $u_{max}(t,\epsilon')$ for $\epsilon' = 10^{-2}$, 10^{-3}, and 10^{-4}. error(t,ϵ') (defined by eq 2.13) is a measure of error in the approximation of the solution of nonlinear equations eq 2.2 by the solution of a linearized problem, given by eq 2.12. $u_{max}(t,\epsilon')$ and ϵ' are defined in the caption of Figure 1.

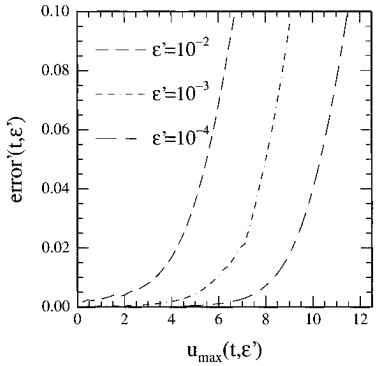

Figure 3. error′(t,ϵ') plotted against $u_{max}(t,\epsilon')$ for $\epsilon' = 10^{-2}$, 10^{-3}, and 10^{-4}. error′(t,ϵ') (eq 2.14b) is a measure of difference between the rescaled solution eq 2.14a of the nonlinear equations eq 2.2 and the rescaled solution of the linearized problem, given by eq 2.12.

the interface with a slightly larger opening. This causes a difference in the resisting pull-out force between the chains in this region and those outside. This difference in the resisting pull-out force is greater for interface 1, as the number of entanglements in interface 1 is larger than that of interface 2 (for the same change in opening displacement), thus decreasing the maximum opening displacement for localization for interface 1.

3.1.3. Comparison with Linear Stability Analysis. Additional insight into the evolution of the interface opening may be obtained by comparing the solution of the nonlinear problem with the solution of the linearized problem u^{lin}, derived in part 1 of this work. For the interface model considered here, u^{lin} is

$$u^{lin}(t,x) = -(\log(1-t)) + \int_{-\infty}^{\infty} u(0,\kappa) e^{i\kappa x}(1-t)^{|\kappa|}\, d\kappa \tag{2.12}$$

where

$$u(0,\kappa) = \frac{1}{2\pi}\int_{-\infty}^{\infty} u(0,x) e^{-i\kappa x}\, dx$$

These equations follow from eq 1.33a and from the fact that for elastic half-space $\lambda(\kappa) = -|\kappa|$.

The solution of the linearized problem eq 2.12 may be directly compared with the solution of the fully nonlinear equations, with an error calculated according to

$$\text{error}(t,\epsilon') = \frac{\max_x |u^{lin}(t,x) - u(t,x)|}{\max_x(u(t,x)) - \min_x(u(t,x))} \tag{2.13}$$

Note that error(t,ϵ') depends on initial conditions. Figure 2 shows plots of error(t,ϵ') vs $u_{max}(t,\epsilon')$ for different values of ϵ'. As expected, the smaller ϵ' is, the better is the approximation of the nonlinear solution by the linearized one. This is in agreement with the fact that small ϵ' corresponds to a small amplitude of the initial perturbation from the homogeneous solution so that spatial inhomogeneities take longer to develop. Note that significant errors occur before localization starts to develop, as is evident by comparing the cases of $\epsilon' = 10^{-2}$ and 10^{-3} on Figures 1 and 2. For example, for $\epsilon' = 10^{-3}$, error(t,ϵ') reaches 10% when $u_{max}(t,\epsilon') \approx 4.5$, while the maximum opening displacement at the onset of localization, $u_c(\epsilon')$, is approximately 10.

3.1.4. Scaling between the Linear and Nonlinear Solutions. In our simulation, we observed that the linearized solution eq 2.12 remains qualitatively similar to the nonlinear solution even after error(t,ϵ') becomes significant. To express this observation quantitatively, we rescale the solution $u(t,x)$ by

$$\hat{N}(u(t,x)) = \frac{u(t,x) - \min_x(u(t,x))}{\max_x(u(t,x)) - \min_x(u(t,x))} \tag{2.14a}$$

The rescaling of $u(t,x)$ corresponds to a rigid translation by $\min_x(u(t,x))$ and a uniform stretch by the factor of $1/[\max_x(u(t,x)) - \min_x(u(t,x))]$.

According to eq 2.14a, $\hat{N}(u(t,x))$ is a function with values between 0 and 1. Our numerical result in Figure 3 indicates that

$$\text{error}'(t) \equiv \max_x |\hat{N}(u(t,x)) - \hat{N}(u^{lin}(t,x))| \tag{2.14b}$$

remains small even after error(t,ϵ') becomes significant. This means that in the beginning of the instability development, the deviation of the linearized solution from the exact solution is due to a rigid body translation and a uniform stretch. In other words, the initial deviation between linear and nonlinear solutions is not due to localization, which forms later in the instability process. Note that the dependence of error′(t) on ϵ' is not explicitly included in the notation in eq 2.14b. Figure 3 shows a plot of error′(t) vs $u_{max}(t,\epsilon')$ for different values of ϵ'. Comparison of Figures 1 and 3 shows that the values of $u_{max}(t,\epsilon')$ corresponding to the beginning of the localization are approximately the same as those corresponding to the moment when error′(t) starts to grow. For example, for the case of $\epsilon' = 10^{-3}$, localization starts to develop when $u_{max}(t,\epsilon') \approx 10$ (Figure 1) and error′(t) reaches 10% when $u_{max}(t,\epsilon') \approx 9$.

3.2. Crack Formation, $u \geq A$. We study how interface failure depends on the amplitude of the initial perturbation ϵ and A. The original equations, eqs 2.2a,b, were integrated using procedure 2 described above. In this set of simulations, the amplitude of the initial perturbation was measured by ϵ instead of ϵ', because ϵ is directly related to the amplitude of the initial opening in the physical system eq 1.24d. The same shape of the initial noise was used in all the simulations in this section. The integration was stopped after the total failure of the interface.

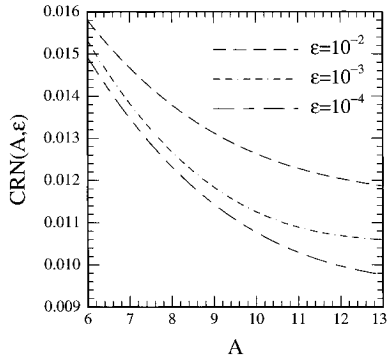

Figure 4. Average number of cracks per unit dimensionless interface area CRN(A,ϵ) (defined by eq 2.16) plotted as a function of A for $\epsilon = 10^{-2}$, 10^{-3}, and 10^{-4}. ϵ is the physical amplitude of the initial perturbation in the interface opening defined by eq 1.24d. A is proportional to the entanglement number of the pull-out chains and is defined by eq 1.23a.

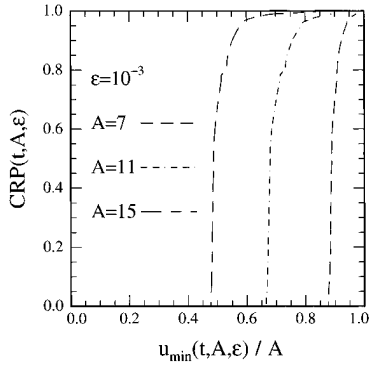

Figure 5. Cracked portion of the interface as a function of time, CRP(t,A,ϵ) (defined by eq 2.15) is plotted vs $u_{\min}(t,A,\epsilon)/A$. $u_{\min}(t,A,\epsilon)$ is the minimum value of the interface opening, defined by eq 2.17, for $A = 7$, 11, and 15 and $\epsilon = 10^{-3}$.

In the following, we introduce three new quantities CRP(t,A,ϵ), CRN(A,ϵ), and $u_{\min}(t,A,\epsilon)$ to describe the dependence of the failure modes on the parameters ϵ and A.

The cracked portion of the interface as a function of time, CRP(t,A,ϵ), is defined as the ratio of the interface area occupied by cracks to the total area:

$$\mathrm{CRP}(t,A,\epsilon) = \frac{\int_0^L \theta(u(t,x) - A)\,\mathrm{d}x}{L} \qquad (2.15)$$

where

$$\theta(y) = \begin{cases} 1, & y \geq 0 \\ 0, & y < 0 \end{cases}$$

The function CRP(t,A,ϵ) depends on parameters ϵ and A.

The average number of cracks per unit area CRN(A,ϵ) is defined as the integral of the number of cracks per unit normalized area of the interface with respect to the cracked portion of the interface:

$$\mathrm{CRN}(A,\epsilon) = \int_0^1 \frac{(\text{no. of crack in } L)}{L} \frac{\partial CRP(t,A,\epsilon)}{\partial t}\,\mathrm{d}t \qquad (2.16)$$

In other words, CRN(A,ϵ) is the area under the curve which results from plotting the number of cracks per unit area of the interface vs the cracked portion of the interface. CRN(A,ϵ) also depends on the shape of initial noise, but for sufficiently large L, this dependence is weak, and since we use the same shape of initial noise $\tilde{g}(x_i)$, $1 \leq i \leq N$, in all simulations, we do not indicate this dependence explicitly. Note that 1/CRN(A,ϵ) is the characteristic mean spacing between cracks. This observation is important for the interpretation of numerical results, as we shall see below.

Finally, we define the minimum value of the interface opening by

$$u_{\min}(t,A,\epsilon) \equiv \min_x(u(t,x;A,\epsilon)) \qquad (2.17)$$

This quantity is used to characterize the inhomogeneity of the interface opening during the fracture process.

One important characteristic feature of the fracture process is the normalized density of cracks or, equivalently, the characteristic normalized distance between cracks 1/CRN(A,ϵ). Figure 4 shows how the average number of cracks per unit dimensionless interface area CRN(A,ϵ) depends on A and ϵ. Note that the general trend is the normalized density of cracks decreases as A increases or ϵ decreases. This figure shows that the dependence of CRN(A,ϵ) on ϵ is weak compared with the dependence on A. Since $A = C\Delta = \mu s/s_e$, the material parameter which has a significant effect on the failure mode (i.e., density of cracks) is the entanglement number s/s_e of the pull-out chains. It is important to note that since the spatial coordinate x is normalized, the characteristic distance between cracks in the physical system depends on the quantities involved in this normalization. For example (see eq 2.3), the normalization of the spatial coordinate depends on the level of applied load, i.e., $x' \propto x\sigma_\infty$. Thus, the actual physical crack spacing depends inversely on the applied load and decreases as the applied load increases; i.e., the crack density increases as applied load is increased. To study the dependence of the physical crack spacing on A, we observe that, according to eq 2.3, $x' \approx 15\sigma_\infty(1 - \nu)/(8\sqrt{K_A}s_eG)x$. For a rubberlike network, $G \propto 1/s_e$ so that neither s nor s_e is involved in the normalization of the spatial coordinate. This means that the dependence of the physical crack spacing on the entanglement number of pull-out chains is qualitatively the same as that of the normalized crack spacing, which is shown in Figure 4. Another important characteristic of the fracture process is how inhomogeneous the interface opening is during fracture. To obtain some insight, we plot CRP(t,A,ϵ) vs $u_{\min}(t,A,\epsilon)/A$ for different values of A with $\epsilon = 10^{-3}$ in Figure 5. This figure shows that the curves with different values of A exhibit the same qualitative feature: after the initiation of the first crack, CRP(t,A,ϵ) reaches about 90%, while $u_{\min}(t,A,\epsilon)$ stays almost constant. The rest of the time is spent on pulling out the remaining 10% of the chains, which makes little contribution to the area occupied by cracks. On the other hand, Figure 5 shows that the value of $u_{\min}(t,A,\epsilon)/A$ corresponding to the beginning of the fracture is strongly dependent on A: it decreases monotonically with A. This figure shows that for $A = 7$, the first crack is formed when the interface opening everywhere reaches about 90% of the critical value so that the interface fails almost homogeneously. On the other hand, the interface opening displacement in some regions is below 50% of the critical value ($u_{\min}(t,A,\epsilon)/A < 0.5$) when the first crack is formed for the case of $A = 15$. Even when 90% of the interface fails (CRP(t,A,ϵ) reaches about 90%), the displacement in the pull-out regions where $u_{\min}(t,A,\epsilon)/A < 0.5$ remains practically unchanged. The final fracture of the interface proceeds by the pull-out of chains in these intact regions. Thus, for $A = 15$, the fracture process is very inhomogeneous.

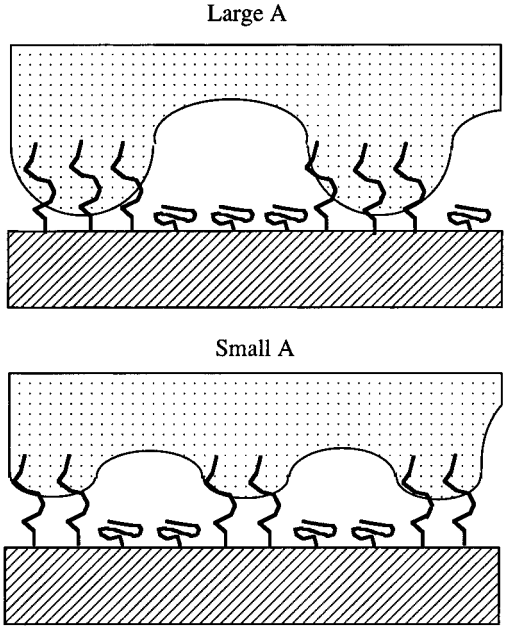

Figure 6. Dependence of the fracture process on A illustrated schematically. A is proportional to the entanglement number of pull-out chains and is defined by eq 1.23a.

As pointed out earlier (see Figure 4), the dependence of the fracture process on ϵ is relatively weak compared with that on A. The dependence of the fracture process on A is schematically illustrated in Figure 6. The general trend is that longer pull-out chains (larger A) lead to a sparser set of cracks, which are more "deep" in the sense that the minimum interface opening is small relative to the critical value Δ when cracks initiate (i.e., the maximum over the uncracked portion of the interface of the imbedded portion of the chain length is large). In contrast, short pull-out chains result in a more dense and "shallow" crack pattern.

4. Conclusion

A numerical procedure was developed to simulate the deformation and failure of an interface reinforced by chains.

We first simulated the development of instability which leads to spatial localization of the interface. These simulations demonstrate that the linear instability predicted in part 1 leads to the development of the spatial localization of the interface deformation. Our results show that as the entanglement number of pull-out chains or the amplitude of the initial perturbation increases, the maximum relative opening displacement δ/Δ needed to develop spatial localization decreases. Our numerical results show that the instability predicted by the linearized solution in part 1 deviates significantly from the solution of the nonlinear equations before the development of spatial localization. However, we demonstrated that the nonlinear solution in this regime (before localization) can be approximated by a rigid translation and a uniform stretching of the linearized solution.

We next studied the failure of the interface by the nucleation and propagation of interface cracks. Our analysis showed that the average crack density increases with the amplitude of the initial perturbation ϵ and decreases with the entanglement number of the pull-out chains s/s_e. The dependence of the average crack density on ϵ is much weaker than its dependence on s/s_e. Likewise, the failure mode of the interface is much more sensitive to s/s_e than it is to ϵ. For small values of A or s/s_e, the interface fails in a homogeneous manner; i.e., right after crack initiation, the interface opening displacement reaches about 90% of the critical value everywhere on the interface. On the other hand, for large entanglement number s/s_e, the interface fails in a very inhomogeneous manner in the sense that right after crack initiation, there are regions of the interface with opening displacement less than 50% of the critical value. In this case, even when 90% of the interface has failed, there are still a few intact regions with opening displacement well below the critical level. The ultimate failure of the interface proceeds by the pull-out of chains in these intact regions.

Acknowledgment. C.-Y. Hui is supported by the Materials Science Center at Cornell, which is funded by the National Science Foundation (DMR−MRL Program). We acknowledge Professor E. J. Kramer for valuable comments and discussions.

Appendix

We conducted a test for size effect. This test allow us to determine N and L used in our numerical procedure. In this test, $\epsilon' = 10^{-1}$. Three separate simulations with $L = L_t$, L_l, and L_r were performed. First, we set $L = L_t = 64(2\pi) = 64(2\pi)/\kappa_c$ (recall that the critical normalized wavelength for instability is 2π; i.e., $\kappa_c = 1$), $N_t = 1024$, and $\Delta x = L_t/N_t$. The initial perturbation $\tilde{g}_t(x_i)$, $1 \le i \le N_t$, is obtained by the generation of white noise. In the first simulation, the interval of periodicity is equal to L_t, the mesh contains N_t nodes, and the initial conditions are given by $\epsilon'\tilde{g}_t(x_i)$. The parameters $(L_l, N_l, \tilde{g}_l(x_i))$ and $(L_r, N_r, \tilde{g}_r(x_i))$ used in the other two simulations are given by

$$L_l = L_r = L_t/2$$

$$N_l = N_r = 512 = 1024/2$$

$$\tilde{g}_l(x_i) = \tilde{g}_t(x_i) \quad 1 \le i \le N_l$$

$$\tilde{g}_r(x_{i-N_r}) = \tilde{g}_t(x_i) \qquad N_r + 1 \le i \le N_t$$

In other words, we devided the interval L_t into two parts and treated each part as independent. All three simulations are performed using procedure 1 and are stopped at the same time T, which is defined by $u^t_{max}(T,\epsilon') = 10$, where u^t is the solution of the simulation using L_t with initial conditions $\epsilon'\tilde{g}_t(x_i)$. To check for the presence of size effect, we compare $u^t(T,x_i)$, $1 \le i \le N_l$, with $u^l(T,x_i)$, $1 \le i \le N_l$, and $u^t(T,x_i)$, $N_r + 1 \le i \le N_t$, with $u^r(T,x_{i-N_r})$, $N_r + 1 \le i \le N_t$, where u^l and u^r are the solutions with initial conditions $\epsilon'\tilde{g}_l(x_i)$ and $\epsilon'\tilde{g}_r(x_i)$, respectively. The agreement between these solutions is excellent. We thus conclude that size effects in the simulation are negligible if the parameters $L = 64\pi$ and $N = 512$ are used. This choice of L and N allows us to approximate an infinite interface by a finite one. To improve accuracy, all simulations are performed for $L = 32(2\pi)$ and $N = 1024$ (the number of nodes was increased to provide better accuracy for the simulations of crack propagation).

References and Notes

(1) Kogan, L.; Hui, C.-Y.; Ruina, A. *Macromolecules*, preceding paper in this issue.

MA950908N